RSC Sustainability

ROYAL SOCIETY OF CHEMISTRY

PAPER

View Article Online
View Journal | View Issue

Cite this: *RSC Sustainability*, 2025, **3**, 4785

Disaccharides as substrates and mechanistic probes for efficient carbohydrate conversion to formic acid in water near room temperature

Stefan S. Warthegau, † Mette-Maya Siewertsen, † Robert Madsen and Sebastian Meier *

Formate is a hydrogen carrier that can be obtained by the oxidation of carbohydrates with hydrogen peroxide under aqueous alkaline conditions near room temperature. The most relevant route among various conceivable pathways for glucose degradation has only recently been clarified. The conversion of biomass-derived disaccharides such as maltose from starch and cellobiose from cellulose into formate could further support the green production of formate. The mechanism, intermediates, side products, and effect of the substrate structure (such as α- *vs.* β-linkages or the presence of reducing *vs.* non-reducing ends) remain poorly understood for the conversion of *O*-glycosidically linked carbohydrates. Here, we close these gaps and show that stoichiometric amounts of base and a surplus of hydrogen peroxide can lead to a near-quantitative and surprisingly rapid conversion of disaccharides to >97% organic carbon in formate. Real-time observations show that glucose is the main intermediate, indicating that the accessibility of the aldehyde groups in stable glucopyranosyl rings is a limiting factor. Side products include glycosylated aldonic acids, which derive from aldose-to-ketose isomerization near the reducing end. This transformation, known as the Lobry de Bruyn–Van Ekenstein transformation, facilitates partial oxidation pathways leading to stable glycosylated **C10** and **C11** acids. Higher concentrations of H_2O_2 suppress isomerization by favoring direct oxidative cleavage, thus minimizing these side products. The absence of disaccharide byproducts, the near-complete conversion of reducing and non-reducing glucopyranosyl residues in disaccharides, and the effect of radical scavengers provide further mechanistic understanding. The combination of quantitative NMR, isotope labeling, and real-time reaction tracking thus provides novel insight into the efficient conversion of disaccharides to formate.

Received 15th July 2025
Accepted 18th August 2025

DOI: 10.1039/d5su00588d

rsc.li/rscsus

Sustainability spotlight

Rising levels of anthropogenic CO_2 underscore the need for sustainable energy storage and transport solutions. Nature remains exceptionally efficient in the capture of CO_2 by photosynthesis, storing both carbon and hydrogen in carbohydrates. Our study seeks to efficiently use natural resources by converting carbohydrates such as cellobiose (from cellulose) and maltose (from starch) to formic acid as a source of hydrogen and a clean energy carrier. This approach supports several UN Sustainable Development Goals, including affordable and clean energy (SDG 7) and climate action (SDG 13) by using biomass-sourced substrates and providing a low-energy alternative for hydrogen production. The process achieves exceptional selectivity near room temperature and aligns with SDG 12 (responsible consumption and production) through efficient resource use.

Introduction

The oxidative conversion of biomass is an important means to produce many industrially relevant chemicals.[1–6] Emerging processes for the oxidative conversion of biomass include the depolymerization of lignin,[7–9] the oxidation of carbohydrates[3,10–14] and furanic compounds[2,5,15–18] to carboxylic acids, and oxidative double bond cleavage in fatty acids.[19–24] It has been pointed out that many, if not most, chemicals sourced from petroleum can also be synthesized from biomass.[19] For oxidative conversions of biomass, an alternative to gaseous oxygen as the oxidant is liquid hydrogen peroxide, which is widely recognized as a green oxidant for research and industrial uses.[4,19] The use of hydrogen peroxide in effective and selective conversions of abundant substrates such as lignin, carbohydrates, furanic derivatives and fatty acids has been reported.[19] However, the exact conversion pathways often remain incompletely understood, and the lack of mechanistic clarity limits strategies to optimize desired reaction outcomes.

Department of Chemistry, Technical University of Denmark, Kemitorvet, Building 206, 2800 Kgs Lyngby, Denmark. E-mail: semei@kemi.dtu.dk

† Equal contribution.

Carbohydrates produced during photosynthesis store both carbon and hydrogen. Hence, carbohydrates are prospective sources of hydrogen, a clean energy carrier.[25] An alternative to energy-intensive processes for producing hydrogen is the conversion of carbohydrates to formic acid as a safe-to-handle liquid-phase hydrogen-storage material that readily releases hydrogen.[26–31] Formate is thus a prospective bulk material for synthetic and energy applications, and its formation attracts increasing interest due to increasing availability of hydrogen peroxide and interest in biomass conversion.[14,32] Mechanistic pathways in the conversion of carbohydrates pose particular problems and remain frequently controversial due to the presence of various plausible competing pathways and several reactive functional groups.[4,12,13,33] We have recently identified central pathways, unanticipated byproducts, and strategies to optimize the yield in the conversion of monosaccharides to formate.[3] This conversion can be achieved at excellent yield using hydroxides of alkali metals in the presence of hydrogen peroxide close to room temperature.[11,34,35]

The functional interaction between reactive oxygen species and biomolecules bears relevance not only for sustainable production, but also for biology, as reactive oxygen species can induce the degradation of polysaccharides and affect their bioactivities.[36–39] Considering the action of reactive oxygen species in the degradation of polysaccharides, *O*-glycosidically linked carbohydrates have also been considered attractive targets for the conversion of biomass to formate.[4,40,41] Encouraged by the recent clarification of monosaccharide degradation pathways to formate, we hypothesized that a combination of isotope tracking using [1′-^{13}C]cellobiose (β-D-[1-^{13}C]glcp-(1→4)-D-glc), quantitative NMR for non-selective observations, and real-time reaction tracking could improve insights into the conversion of *O*-glycosidically linked carbohydrates. Insight into suitable reaction conditions, intermediates, rates, byproducts, pathways, and mechanisms for the conversion of biomass-derived substrates such as maltose from starch and cellobiose from cellulose was hence pursued herein. Under optimized conditions, formate could account for more than 97% of the organic carbon obtained from cellobiose. Various mechanisms for the cleavage of the carbohydrate backbone from the reducing end have previously been described (Scheme 1) and differ in their respective reaction outcomes when using cellobiose as a probe molecule. The isotope label in [1′-^{13}C]cellobiose showed that [1-^{13}C]glucose was the principal intermediate towards ^{13}C formate, indicating that the accessibility of the aldehyde groups in stable glucopyranosyl rings is limiting. Formate derived from [1′-^{13}C]cellobiose incorporated approximately 8.7% more ^{13}C than formate formed from natural abundance cellobiose, consistent with the formation of formate from all 12 different positions in cellobiose, with no indication that the degradation stalls at shorter disaccharides (Scheme 1).

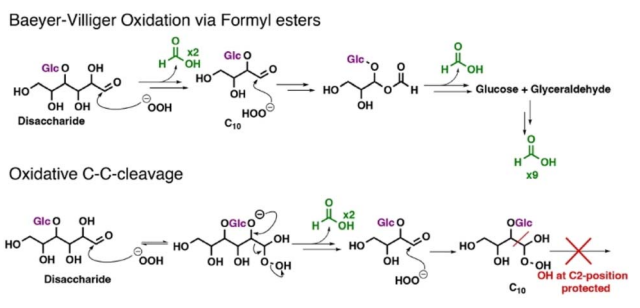

Scheme 1 Possible pathways in the conversion of reducing carbohydrates using alkaline hydrogen peroxide solutions, either *via* formyl esters or *via* oxidative C–C cleavage, leading to different anticipated product compositions.

Results and discussion

Selectivity in cellobiose conversion

Cellobiose was chosen as the main substrate in this study as the disaccharide is released from cellulose by cellobiohydrolases and as its isotope-labelled form is commercially available. Initially, cellobiose (50 mM) was converted in 0.6 M LiOH[3,14] with stoichiometric amounts of hydrogen peroxide or in the presence of a surplus of hydrogen peroxide (2 and 3 equiv. on a carbon basis relative to the **C12** compound cellobiose). Using 1.8 M hydrogen peroxide (3 equiv. per substrate carbon) led to a product mixture containing nearly pure formate after conversion for 24 h at 308 K (Fig. 1A). Quantitative determinations were conducted using 1D ^{1}H NMR with an inter-scan

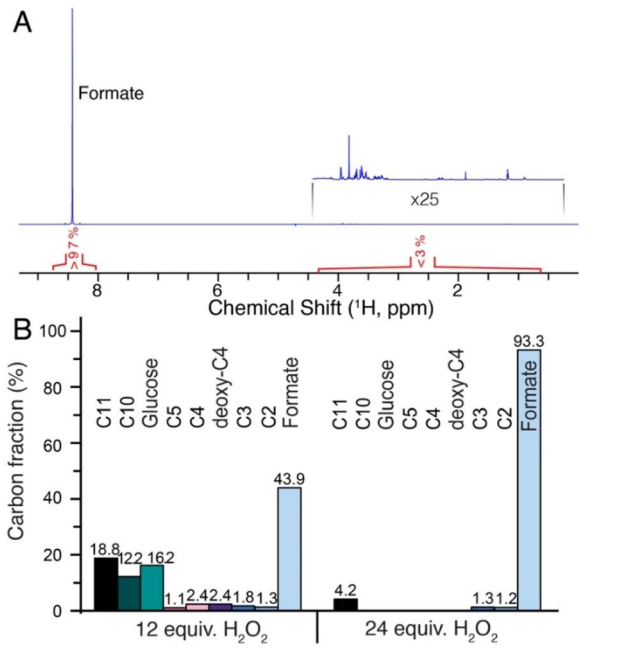

Fig. 1 (A) Quantitative ^{1}H NMR spectrum for determining the organic composition after the conversion of cellobiose in aqueous alkaline hydrogen peroxide with 36 equiv. (3 equiv. per substrate carbon) hydrogen peroxide. (B) Carbon fractions for aldonic acids in addition to glucose at lower oxidant concentrations. **C11** and **C10** correspond to *O*-glycosylated **C5** and **C4** aldonic acids, respectively. Reaction conditions: 0.05 M cellobiose, 0.6 M LiOH and variable equiv. hydrogen peroxide (36 in (A) and 12 and 24 in (B)) in a 1.5 mL Eppendorf tube (200 μL H_2O/D_2O (90%/10%)) at 308 K, shaken at 600 rpm for 24 h.

recycle time duration of 25 s for data acquisition and relaxation. Subsequent optimization indicated that inter-scan relaxation delays of approximately 5 s could suffice for full recovery of the formate signal for quantitative measurements (Fig. S1). This comparably short time for full recovery of the formate ^{1}H NMR signal[42] was consistent with an expected acceleration of relaxation in the presence of paramagnetic species such as oxygen and related species.

Having established a quantification method for formate using qNMR, the carbon balance of formate and side products was approximated from the quantitative ^{1}H NMR signal. The number of aliphatic hydrogens reflects the number of carbons both in aldonic acids (*e.g.* two carbons and two aliphatic hydrogens in glyoxylate) and aldoses (*e.g.* six carbons and six non-anomeric aliphatic hydrogens in glucose). Hence, qNMR indicates that the experiment of Fig. 1A corresponds to a balance of organic carbon of more than 97% in formate and less than 3% in side products.

Side products were separately identified for the experiment converting cellobiose (50 mM) in the presence of 0.6 M hydrogen peroxide (12 equiv.) and 0.6 M LiOH for 24 h (Fig. 1B). The main side products included glycosides of aldonic acids shortened from the reducing end. Thus, 3-glycosylated arabinonate and 2-glycosylated erythronate (designated **C11** and **C10** in Fig. 1B) were formed from cellobiose. Molecular species with shortened sugars at the reducing end were not detected. These findings parallel previous observations in the formation of aldonic acid byproducts when using glucose as the substrate, where shortened aldoses reacted faster than glucose and did not accumulate.[3] Aldonic acids are plausible products formed upon the cleavage of ketoses formed from the Lobry de Bruyn–Van Ekenstein transformation of the reducing end carbohydrate to its corresponding ketose (Fig. S2). The glycosidic bond to arabinonate and to erythronate could evidently withstand the reaction conditions. The **C11** and **C10** compounds of Fig. 2 were found to account for up to 30% of the carbon balance when converting the **C12** substrate cellobiose with 12 equiv. hydrogen peroxide per substrate, while increasing hydrogen peroxide amounts favored the formation of formate over organic side products. Thus, the carbon fraction of side products declined to less than 7% in the presence of 24 equiv. hydrogen peroxide (Fig. 1B) and to less than 3% in the presence of 36 equiv. hydrogen peroxide (Fig. 1A). The isomerization of the reducing end aldose to its corresponding ketose leads to the emergence of side products of Fig. 2, supported using lactulose (4-*O*-β-D-galactosyl-D-fructose) as the substrate with a ketose at the reducing end. Here, *O*-glycosylated arabinonate alone accounted for 47% of the carbon balance (Fig. S3).

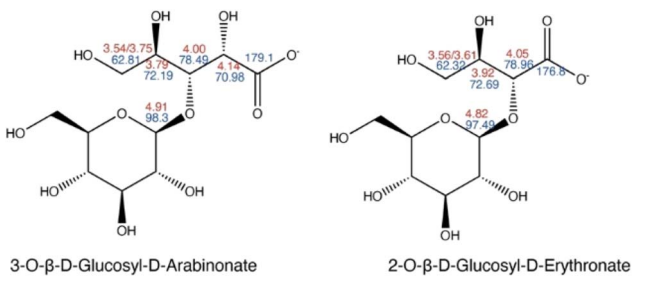

Fig. 2 Side products formed in the conversion of cellobiose in aqueous alkaline hydrogen peroxide.

Effect of reaction conditions on cellobiose conversion and selectivity for formate

Subsequently, we chose to evaluate the effect of reaction parameters on the conversion of cellobiose and the formation of formate in alkaline aqueous solutions of hydrogen peroxide. The substrate concentration was varied from 30 to 70 mM, while keeping the LiOH (0.6 M) and H_2O_2 (1.2 M, 24 equiv.) concentrations constant. As expected, lower concentrations of cellobiose favoured full conversion, while cellobiose was not fully converted at concentrations of 50 mM and above (Fig. 3A).

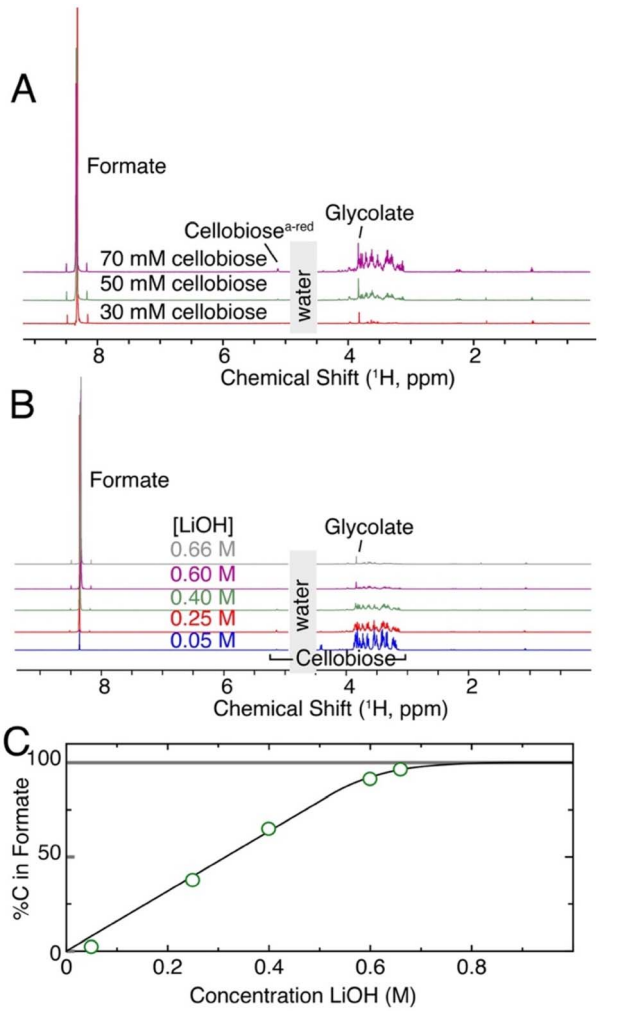

Fig. 3 Product concentration depending on (A) substrate concentration and (B and C) LiOH concentration. The line in (C) is a guide to the eye, and 0.6 M LiOH corresponds to 1 equiv. per substrate carbon. Reaction conditions: (A) variable and (B and C) 0.05 M cellobiose, (A) 0.6 M and (B and C) variable LiOH as indicated and 24 equiv. hydrogen peroxide in a 1.5 mL Eppendorf tube (200 μL H_2O/D_2O (90%/10%)) at 308 K, shaken at 600 rpm for 20 h.

Similarly, a systematic variation of LiOH in the presence of 50 mM substrate and 1.2 M H_2O_2 showed that the yield of formate correlated with the concentration of LiOH, as basic conditions are needed to deprotonate hydrogen peroxide (with a pK_a of 11.6) to the nucleophilic hydroperoxyl anion (HOO^-).[4] While LiOH was selected for comparability with previously reported conditions,[14] it is worth noting that prior studies, including our own work on monosaccharides,[3] indicate that other alkali hydroxides provide similar conversion efficiencies. To experimentally probe alkali hydroxide effects in cellobiose conversion, we conducted a parallel reaction using NaOH under otherwise identical conditions (Fig. S4). The formate yield was comparable to the yield when using LiOH (87% *vs.* 91%). Given its lower cost and widespread industrial use, NaOH would hence likely be the most practical choice for future scale-up. As a result, stoichiometric amounts of base relative to formic acid formed are needed to maintain basic reaction conditions throughout (Fig. 3B and C).

Substrate scope and slower conversion in the absence of the reducing end

To gain insight into the mechanism of conversion of glycosides in an aqueous alkaline solution of hydrogen peroxide, we subsequently used various substrates for conversion and subsequent analysis by qNMR. Initially, maltose (α-D-glcp-(1→4)-D-glc) was used as an alternative substrate to cellobiose (β-D-glcp-(1→4)-D-glc) to evaluate the effect of the glycosidic bond configuration on the conversion and to gain overall insight into the kinetics of disaccharide conversion in aqueous alkaline solutions of hydrogen peroxide. For accurate determination of relative reactivity, maltose and cellobiose were used in a competition experiment containing 25 mM maltose and 25 mM cellobiose, each, in addition to 0.6 M LiOH and 1.2 M hydrogen peroxide. To obtain sufficient signals from the natural abundance substrates, a time series of DEPT135 ^{13}C spectra was implemented as shown in Fig. 4. Opposite to regular decoupled ^{13}C NMR spectra, DEPT135 is enhanced in sensitivity due to the transfer of polarization from protons to carbon. The time course of cellobiose and maltose conversion as tracked *in situ* is plotted in Fig. 4A. The conversion of both disaccharides followed a similar time course with an exponential decay with a half time of approximately 20 min (19.5 and 18.2 min for cellobiose and maltose, respectively) at a reaction temperature of 308 K. Overall, the conversion is rapid and not significantly dependent on the configuration of the glycosidic bond for cellobiose and maltose indicating that linkage stereochemistry (α *vs.* β) has minimal influence on the reaction kinetics under these conditions. Additional experiments at 303 K and 313 K under otherwise identical conditions gave slightly lower, but still acceptable, formate yields (82% and 79%, respectively, Fig. S5). The lower yield at lower temperature may reflect different temperature dependences of C–C cleavage and aldose-to-ketose isomerization, while the lower yield at higher temperature is a plausible consequence of increased thermal decomposition of H_2O_2.

A quantitative ^1H NMR spectrum of products formed from a pure maltose substrate at 50 mM concentration was acquired after conversion at 308 K for 24 h and compared to the product formed from 50 mM cellobiose (Fig. 5). The yield of formate (approximately 84%, 500 mM) and the near-complete

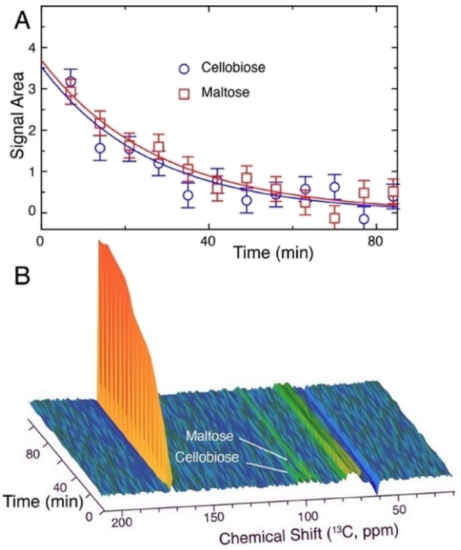

Fig. 4 Competition experiment for the one-pot conversion of maltose and cellobiose. Integrals of the substrates (A) are shown alongside the time series of DEPT135 ^{13}C NMR spectra (B). Reaction conditions: 0.025 M cellobiose and 0.025 M maltose, 0.6 M LiOH and 24 equiv. hydrogen peroxide in a 3 mm NMR tube (200 μL H_2O/D_2O (90%/10%)) at 308 K without agitation.

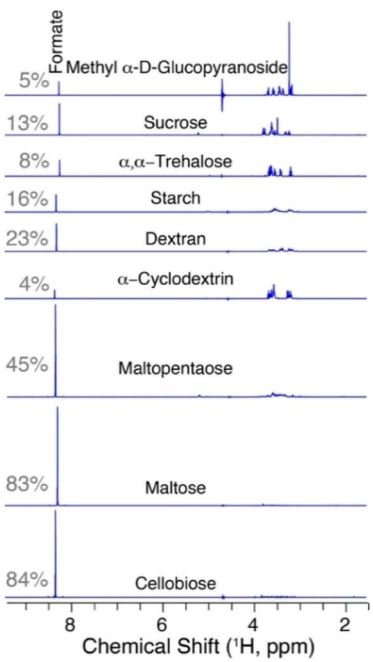

Fig. 5 Quantitative ^1H NMR spectra upon the conversion of various substrates under identical conditions, showing lower, but detectable, formate yields from non-reducing carbohydrates (grey fractions to the left). Reaction conditions: a concentration corresponding to 0.1 M glucose monomer, 0.6 M LiOH and 24 equiv. hydrogen peroxide in a 1.5 mL Eppendorf tube (200 μL H_2O/D_2O (90%/10%)) at 308 K, shaken at 600 rpm for 20 h.

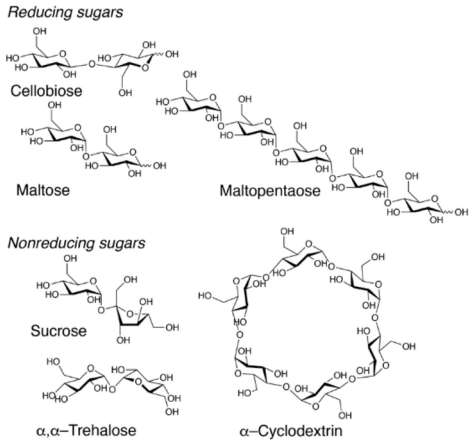

Scheme 2 Di- and oligosaccharides that were used as substrates.

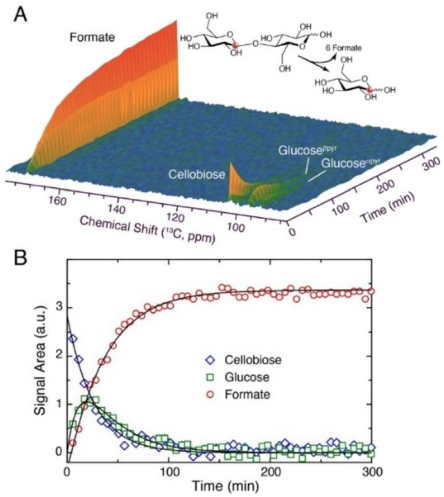

Fig. 6 Real-time observation of the conversion. Reaction conditions: 0.05 M [1′-^{13}C]cellobiose, 0.6 M LiOH and 24 equiv. hydrogen peroxide in a 3 mm NMR tube (200 μL H_2O/D_2O (90%/10%)) at 308 K without agitation.

conversion of disaccharide were similar for both 1,4-glucopyranosyl-glucoses, as expected from the behavior in real time reaction tracking.

Other water soluble di-, oligo- and polysaccharides were subsequently used as substrates (Scheme 2) to evaluate the effect of glycosidic linkages and the fraction of the reducing end on the product composition. All substrates were used at a concentration corresponding to 100 mM monomer. Maltopentaose is a reducing pentasaccharide and yielded 45% (270 mM) formate. By contrast, the cyclic α-1,4 linked hexasaccharide α-cyclodextrin showed only small (4%, 24 mM), albeit non-negligible conversion to formate. These observations indicated that degradation predominantly proceeds from the reducing end, while internal scission of glycosidic bonds or C–C bonds is substantially slower. This trend was substantiated using the non-reducing α,α-trehalose, sucrose and methyl α-D-glucopyranoside as substrates. All these non-reducing substrates showed non-complete conversion (anomeric signals and signals near 3–4 ppm in Fig. 5) and a lower carbon fraction in formate (grey numbers in Fig. 5) than reducing carbohydrates, even if the reducing substrates were polymeric such as α-1,6 linked dextran and predominantly α-1,6 linked soluble starch, which highlights the importance of accessible aldehyde termini for efficient degradation to formate. Overall, these results indicated that while internal scissions could occur, the degradation from the reducing end predominated for reducing carbohydrates. The selectivity for formate and the fraction of reducing end in the substrate thus correlated under our chosen reaction conditions (Fig. S6).

Isotope tracking and incorporation into the overall formate pool

Having established the predominant degradation of glycosides from the reducing end, we used [1′-^{13}C]cellobiose (β-D-[1-^{13}C]glc-(1→4)-D-glc) for tracking the reaction and the incorporation of the ^{13}C label into the product. We hypothesized that [1′-^{13}C]cellobiose, which is isotope labelled at the anomeric carbon in the glycosidic bond, would provide a distinct probe for following the fate of the glycosidic bond. The time series of ^{13}C NMR spectra as shown in Fig. 6A validated the pseudo-first order conversion with a half time near 20 min. The predominant intermediate was free glucose with α- and β-anomeric ^{13}C signals emerging in parallel. Upon further reaction, the ^{13}C label appears in formate as the only main product formed from the anomeric carbon in the glycosidic bond, while over-oxidation yielded 4% carbonate. The kinetics could be fitted to a sequence of irreversible sequential reactions from cellobiose *via* glucose to formate. The respective apparent rate constants for both rate limiting steps were comparable at $k_1 = 0.38$ min^{-1} and $k_2 = 0.11$ min^{-1}. A decline in apparent rate constants for the conversion of first cellobiose and then the glucose intermediate with hydroperoxyl anion seems plausible considering

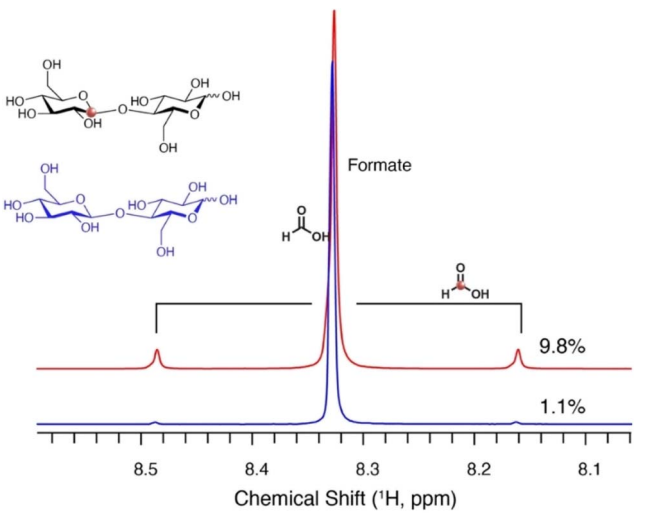

Fig. 7 Reaction conditions: 0.05 M cellobiose or 0.05 M [1′-^{13}C]cellobiose, 0.6 M LiOH and 24 equiv. hydrogen peroxide in a 3 mm NMR tube (200 μL H_2O/D_2O (90%/10%)) after 24 h reaction at 308 K without agitation.

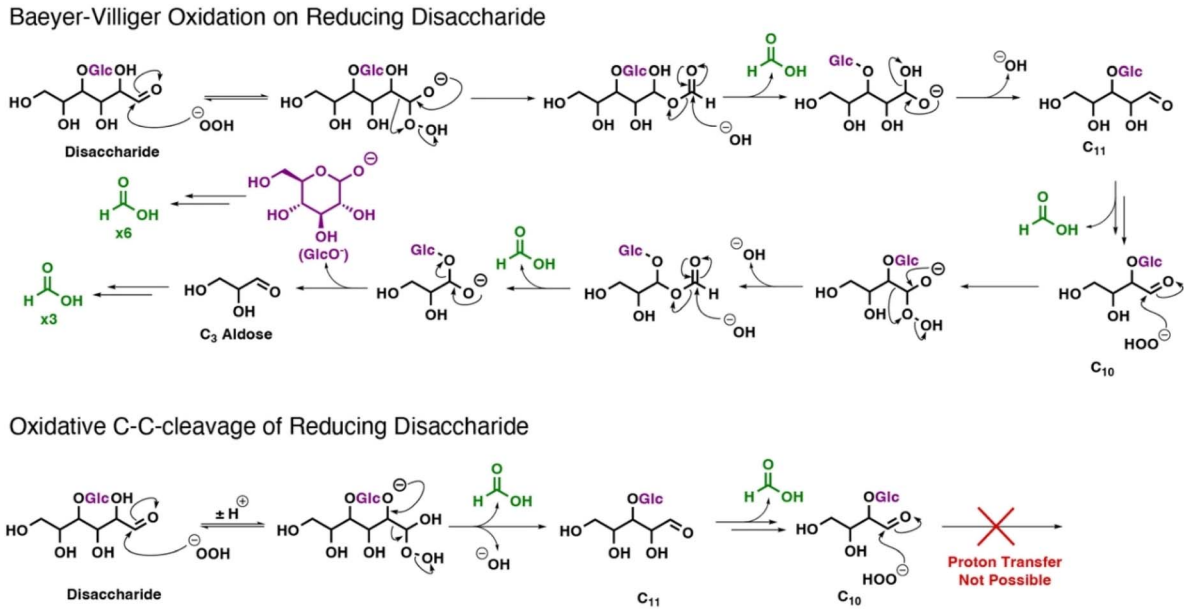

Scheme 3 Plausible mechanisms in the degradation of cellobiose in the presence of a hydroperoxyl anion. The absence of **C10** disaccharide and the rapid and full conversion to formate argue for a central role of Baeyer–Villiger oxidation.

the consumption of hydrogen peroxide and neutralization of some LiOH during reaction progress. The absence of significant non-cellobiose glycosidic signals indicated that a rate limiting step is the opening of the stable glucopyranosyl ring, while subsequent shortening from the reducing end led to faster reactions due to higher accessibility of the aldehyde group upon conversion of the reducing glucopyranosyl moiety. This limited accessibility of the aldehyde group within the closed pyranose ring restricts the initial oxidation step and impacts the efficiency of formate production, particularly for non-reducing disaccharides. The absence of detectable shortened intermediates from cellobiose during reaction tracking reflects observations on product mixtures and is consistent with the increasing accessibility of the aldehyde group.[3]

Quantitative ^{1}H NMR on the product mixture was then used to gain additional mechanistic insight by quantifying the ^{13}C and ^{12}C isotope fractionation in formate (Fig. 7). As expected, the fraction of ^{13}C enriched formate when using natural abundance cellobiose was 1.1%, corresponding to the natural abundance of ^{13}C. By contrast, the fraction of ^{13}C enriched formate formed from [1′-^{13}C]cellobiose was 9.8%. The additional influx of 8.7% ^{13}C into the product is consistent with ^{13}C labelling of one twelfth of the substrate carbons. Overall, isotope tracking thus shows that cellobiose is converted from the reducing end with glucose formed as the intermediate and that carbon atoms from both glucopyranosyl units are converted to formate with high selectivity.

Considering the experimental results, including rapid degradation from the reducing end, complete conversion to formate and the absence of significant shortened disaccharide intermediates or products, we conclude that a Baeyer–Villiger oxidation proceeding *via* unstable formyl esters is a plausible major pathway in the conversion of cellobiose (Scheme 3 top). All observed results are consistent with this pathway. Here, the glycosidic bond is broken as an easily hydrolyzed glucosyl hemiacetal of the **C3** aldose glyceraldehyde. By contrast, oxidative C–C cleavage depends on the presence of a hydroxyl group adjacent to the carbonyl that is liberated in the oxidized form. This mechanism would imply that degradation stalls due to the glycosidic linkage. Alternatively, radical reactions are conceivable, but less consistent with the well-defined degradation pathway *via* one main intermediate. The use of TEMPO, which would quench carbon-centered or alkyl radicals, did not prevent the conversion of cellobiose to formate (Fig. S7).[43,44] Nevertheless, the slow degradation of carbohydrates in the absence of a reducing end shows that various pathways are principally accessible in the conversion of *O*-glycosidically linked carbohydrates by aqueous alkaline solutions of hydrogen peroxide.

Conclusion

In conclusion, we find that reducing carbohydrates including cellobiose and maltose can be rapidly converted to formate near room temperature with a half time on the order of 20 min. The carbon fraction of organic side products declined with increasing hydrogen peroxide concentrations. In the conversion of cellobiose, glucose is the main intermediate, and carbons from both glucopyranosyl moieties in the disaccharide get converted to formate with high selectivity. The organic carbon harbored in formate can exceed 97% under suitable conditions. While the absence of a reducing end slows the conversion and reduces selectivity towards formate, spurious reactions to formate are observed for non-reducing sugars. Baeyer–Villiger oxidation could rationalize the complete conversion of cellobiose without dependence on a reaction that cleaves the

glycosidic bond, as an easily hydrolyzed glucosyl hemiacetal forms in this pathway. The absence of glycosylated tetrose products and the absence of significant effects of TEMPO argue against the central relevance of alternative plausible mechanisms, whose principal viability, albeit at slower rates, is witnessed by the reactivity of non-reducing carbohydrates. Overall, isotope tracking and real-time NMR provide novel insight into the conversion of *O*-glycosidically linked carbohydrates to formate, a liquid-phase hydrogen-storage material that is safe to handle. H_2O_2 offers a green and sustainable option that enables complete conversion of reducing disaccharides within just 3 hours, reducing both energy demand and reaction time compared to more forceful oxidative methods.

Experimental section

Chemicals

H_2O_2 (30% w/v) was purchased from Fisher Scientific (Hampton, NH, USA). D_2O (99.9 atom% D), LiOH (98%), D-(+)-cellobiose (≥99.0%), α,α-trehalose dihydrate (≥99.0%), sucrose (≥99.5%), methyl α-D-glucopyranoside (≥99.0%), dextran (analytical standard for GPC, Mw 12 000), maltopentaose, sucrose (≥99.5%), D-(+)-maltose monohydrate (≥99.0%), α-cyclodextrin, and soluble starch (from potato, according to Zulkowsky) were all purchased from Sigma-Aldrich (St. Louis, MO, USA). TEMPO (2,2,6,6-tetramethylpiperidine 1-oxyl radical, ≥96.0%) was from Fluka. [1′-^{13}C]cellobiose (β-D-[1-^{13}C]glcp-(1→4)-D-glc) was purchased from Omicron Biochemicals (South Bend, IN, USA). Deionized water was used in all reactions.

General reaction procedure using a reactor

The standard reaction conditions were conducted on a scale of 200 μL, suitable for analysis using a 3 mm NMR tube. These reactions contained 20 μL carbohydrate solution in D_2O, 35 μL H_2O, 120 μL LiOH stock solution (1 M, H_2O), and 25 μL >30% H_2O_2. The carbohydrate was used at a final monomer concentration of 0.1 M. These conditions correspond to the use of stoichiometric amounts of base per substrate carbon, and 2 equiv. oxidant per substrate carbon due to its beneficial role in suppressing organic byproduct formation. The samples were incubated in a VWR Thermal Shake Lite shaker for 24 h (or the indicated time) at 308 K under agitation at 600 rpm. Reactions of cellobiose were repeated for 5 h in the presence and in the absence of 60 mM TEMPO as a prospective radical scavenger.

General reaction procedure for *in situ* NMR

The standard reaction conditions on a scale of 200 μL also applied to reactions tracked by *in situ* NMR, which typically contained 20 μL carbohydrate solution in D_2O (final concentration 0.1 M), 35 μL H_2O, 120 μL LiOH stock solution (1 M, H_2O), and 25 μL >30% H_2O_2. All reactants were kept on ice and mixed immediately prior to transfer of the reaction mixture to a 3 mm NMR sample tube. The experimental dead time was measured, and an acquisition of a time series of ^{13}C spectra was initiated after tuning and matching, shimming and determination of the ^{1}H 90° pulse.

Quantitative NMR (qNMR)

For accurate quantification of product distributions at a natural isotope abundance, quantitative ^{1}H NMR (qNMR) spectroscopy (*noesypr1d* or *zgesgp* standard pulse sequences) was performed using a relaxation time of 25 s (or variable delays for Fig. S1) between acquisitions in one-dimensional spectra. The *zgesgp* pulse sequence proved to provide valid integrals and better baseline than noesypr1d (10 ms mixing time) for the polyolic signals below 4 ppm. Considering the poor signal recovery of the 1D NOESY experiment especially for short T_1 times,[42] the *zgesgp* pulse sequence was hence used for relative quantifications. The FID was sampled as 16 384 complex data points for 1.7 s while the *d*1 was set to 23.3 s. Product distributions were determined using integrals from these qNMR spectra and accounting for the contribution of equivalent hydrogens to the signals. NMR spectra were acquired using a Bruker (Fällanden, Switzerland) Avance III HD 600 spectrometer equipped with a Bruker Smartprobe and an Ascend Magnet. A total of 16 scans were accumulated in each experiment of 400 s duration. The spectra were processed and integrated using Bruker TopSpin 4.5.

Reaction tracking with *in situ* NMR spectroscopy

In situ NMR spectra using substrates (cellobiose and maltose in a mixture of 25 mM each) at natural isotope abundance were recorded on an 800 MHz Bruker Avance III spectrometer equipped with an 18.7 T magnet and a 5 mm TCI cryoprobe. Time-resolved reaction monitoring was performed using a time series of DEPT135 spectra (*dept135*), implemented as a pseudo-2D experiment. The DEPT135 experiment was chosen to improve the signal to noise ratio relative to a time series of 1D ^{13}C NMR spectra without polarization transfer from hydrogen. Spectra were acquired with a relaxation delay (*d*1 = 1.32 s) that was set to result in a duration of 2.0 s between scans, and 256 transients were accumulated for each FID. The FID sampled 32 768 complex data points during an acquisition time of 0.68 s. For structural elucidation and chemical shift assignment of side products (as shown in Fig. 2), ^{1}H–^{13}C HSQC and HMBC experiments as well as ^{1}H–^{1}H TOCSY experiments were performed on the crude reaction mixture.

Time-resolved reaction monitoring using [1′-^{13}C]cellobiose was performed on a Bruker Avance III HD 600 spectrometer equipped with a Bruker Smartprobe and an Ascend Magnet. A time series of 1D^{13}C NMR spectra (*zgig30*) was implemented as a pseudo-2D experiment. Spectra were acquired with a relaxation delay (*d*1) of 1.5 s between scans, and 160 transients were acquired per FID. The FID sampled 32 768 complex data points during an acquisition time of 1.0 s. Reaction tracking using *in situ* ^{13}C NMR on [1′-^{13}C]cellobiose indicated the conversion of less than 5% of the enriched carbon position to inorganic carbon (carbonate) *via* overoxidation (Fig. S8). A quantitative ^{1}H NMR spectrum was acquired after the reaction to determine the fraction of ^{13}C incorporation into formate.

Data analysis

Data were plotted and fitted using pro Fit 7 (Quantumsoft, Uetikon am See, CH). All spectra were acquired, processed, and

analyzed using Bruker TopSpin 3.5 pl6. Spectra were zero-filled to at least twice the number of complex data points in the FID prior to Fourier transformation.

Conflicts of interest

There are no conflicts to declare.

Data availability

Study data supporting this article have been included as part of the article or SI.

Supplementary information available: dependence of signal recovery on the inter-scan relaxation time; plausible mechanism for formation of O-glycosylated aldonic acid; effect of substrate structure on the product composition; quantitative ^{1}H NMR spectra for determining the organic composition when using varying hydroxides and temperatures; correlation between the initial concentration of reducing end and fraction of organic carbon in formate; effect of TEMPO as a prospective radical scavenger; quantification of ^{13}C label in inorganic carbon. See DOI: **https://doi.org/10.1039/d5su00588d**.

Acknowledgements

This research was funded by the Independent Research Fund Denmark (grant 2035-00119B). NMR data were acquired on instruments of the NMR Center DTU supported by the Villum Foundation.

References

1 Z. Zhang and G. W. Huber, *Chem. Soc. Rev.*, 2018, **47**, 1351–1390.
2 S. S. Warthegau, A. Jakob, M. Karlsson, R. Madsen, M. Grilc, P. R. Jensen and S. Meier, *ACS Catal.*, 2025, 2459–2471.
3 S. S. Warthegau, M.-M. Siewertsen, R. Madsen and S. Meier, *Green Chem.*, 2025, **27**, 8625–8636.
4 S. J. H. F. Arts, E. J. M. Mombarg, H. Van Bekkum and R. A. Sheldon, *Synthesis*, 1997, 597–613.
5 N. Alonso-Fagúndez, I. Agirrezabal-Telleria, P. L. Arias, J. L. G. Fierro, R. Mariscal and M. L. Granados, *RSC Adv.*, 2014, **4**, 54960–54972.
6 R. Behling, S. Valange and G. Chatel, *Green Chem.*, 2016, **18**, 1839–1854.
7 W. Schutyser, J. S. Kruger, A. M. Robinson, R. Katahira, D. G. Brandner, N. S. Cleveland, A. Mittal, D. J. Peterson, R. Meilan, Y. Román-Leshkov and G. T. Beckham, *Green Chem.*, 2018, **20**, 3828–3844.
8 T. Vangeel, W. Schutyser, T. Renders and B. F. Sels, *Top. Curr. Chem.*, 2018, **376**, 30.
9 O. Y. Abdelaziz, I. Clemmensen, S. Meier, C. A. E. Costa, A. E. Rodrigues, C. P. Hulteberg and A. Riisager, *ChemSusChem*, 2022, **15**, e202201232.
10 A. R. E. Hansen, P. R. Jensen and S. Meier, *Catal. Sci. Technol.*, 2023, **13**, 362–371.
11 H. S. Isbell and H. L. Frush, *Carbohydr. Res.*, 1973, **28**, 295–301.
12 H. S. Isbell, H. L. Frush, R. Naves and P. Soontracharoen, *Carbohydr. Res.*, 1981, **90**, 111–122.
13 H. S. Isbell and H. L. Frush, *Carbohydr. Res.*, 1987, **161**, 181–193.
14 C. Wang, X. Chen, M. Qi, J. Wu, G. Gözaydın, N. Yan, H. Zhong and F. Jin, *Green Chem.*, 2019, **21**, 6089–6096.
15 C. Chen, L. Wang, B. Zhu, Z. Zhou, S. I. El-Hout, J. Yang and J. Zhang, *J. Energy Chem.*, 2021, **54**, 528–554.
16 X. Li, B. Ho, D. S. W. Lim and Y. Zhang, *Green Chem.*, 2017, **19**, 914–918.
17 H. Zhang, S. Wang, H. Zhang, J. H. Clark and F. Cao, *Green Chem.*, 2021, **23**, 1370–1381.
18 S. S. Warthegau, M. Karlsson, P. R. Jensen and S. Meier, *Chem. Commun.*, 2025, **61**, 3680–3683.
19 S. P. Teong, X. Li and Y. Zhang, *Green Chem.*, 2019, **21**, 5753–5780.
20 U. Biermann, U. T. Bornscheuer, I. Feussner, M. A. R. Meier and J. O. Metzger, *Angew. Chem., Int. Ed.*, 2021, **60**, 20144–20165.
21 B. M. Stadler, C. Wulf, T. Werner, S. Tin and J. G. De Vries, *ACS Catal.*, 2019, **9**, 8012–8067.
22 A. E. Kerenkan, F. Béland and T.-O. Do, *Catal. Sci. Technol.*, 2016, **6**, 971–987.
23 Z. Zhou, Y.-L. Li, F. Zhao, R. Xin, X.-H. Huang, Y.-Y. Zhang, D. Zhou and L. Qin, *J. Agric. Food Chem.*, 2022, **70**, 16410–16423.
24 A. Soutelo-Maria, J.-L. Dubois, J.-L. Couturier and G. Cravotto, *Catalysts*, 2018, **8**, 464.
25 K. Sharma, *Renew. Sustain. Energy Rev.*, 2019, **105**, 138–143.
26 K. Liu and Y. Li, *ACS Appl. Mater. Interfaces*, 2024, **16**, 62033–62042.
27 Q. Sun, N. Wang, Q. Xu and J. Yu, *Adv. Mater.*, 2020, **32**, 2001818.
28 A. Léval, A. Agapova, C. Steinlechner, E. Alberico, H. Junge and M. Beller, *Green Chem.*, 2020, **22**, 913–920.
29 M. Navlani-García, K. Mori, D. Salinas-Torres, Y. Kuwahara and H. Yamashita, *Front. Mater.*, 2019, **6**, 44.
30 X. Yu and P. G. Pickup, *J. Power Sources*, 2008, **182**, 124–132.
31 D. A. Bulushev, *Energies*, 2021, **14**, 1334.
32 L. Wu, Y. Yang, J. Cheng, X. Shi, H. Zhong and F. Jin, *ACS Sustain. Chem. Eng.*, 2022, **10**, 15423–15436.
33 H. S. Isbell, *Carbohydr. Res.*, 1976, **49**, C1–C4.
34 H. S. Isbell, H. L. Frush and E. T. Martin, *Carbohydr. Res.*, 1973, **26**, 287–295.
35 G. J. Moody, in *Advances in Carbohydrate Chemistry*, ed. M. L. Wolfrom, Academic Press, 1964, vol. 19, pp. 149–179.
36 Y. Dai, C. Shao, Y. Piao, H. Hu, K. Lu, T. Zhang, X. Zhang, S. Jia, M. Wang and S. Man, *Carbohydr. Pol.*, 2017, **178**, 34–40.
37 X. Chen, D. Sun-Waterhouse, W. Yao, X. Li, M. Zhao and L. You, *Food Chem.*, 2021, **365**, 130524.
38 V. Maksimović, M. Mojović and Ž. Vučinić, *Carbohydr. Res.*, 2006, **341**, 2360–2369.
39 J.-F. Cui, S. Bystroem, P. Eneroth and I. Bjoerkhem, *J. Org. Chem.*, 1994, **59**, 8251–8255.
40 J.-H. Park, D.-W. Lee, M.-H. Jin, Y.-J. Lee, G.-S. Song, S.-J. Park, H. J. Jung, K. K. Oh and Y.-C. Choi, *Chem. Eng. J.*, 2021, **421**, 127827.
41 J. Yun, G. Yao, F. Jin, H. Zhong, A. Kishita, K. Tohji, H. Enomoto and L. Wang, *AIChE J.*, 2016, **62**, 3657–3663.

42 A. R. E. Hansen, K. Enemark-Rasmussen, F. A. A. Mulder, P. R. Jensen and S. Meier, *J. Phys. Chem. C*, 2022, **126**, 11026–11032.
43 B. M. Ali, M. Boothapandi and A. Sultan Nasar, *Data Brief*, 2020, **28**, 104972.
44 W. G. Skene, J. C. Scaiano, N. A. Listigovers, P. M. Kazmaier and M. K. Georges, *Macromolecules*, 2000, **33**, 5065–5072.